High performance aptasensing platform development through in silico aptamer engineering for aflatoxin B1 monitoring

High performance aptasensing platform development through in silico aptamer engineering for aflatoxin B1 monitoring

Maryam Mousivand, Mohammad Javan-Nikkhah, Laura Anfossi, Fabio Di Nardo, Matteo Salina, Kowsar Bagherzadeh

PII: S0956-7135(22)00611-9

DOI: https://doi.org/10.1016/j.foodcont.2022.109418

Reference: JFCO 109418

To appear in: *Food Control*

Received Date: 12 June 2022

Revised Date: 10 September 2022

Accepted Date: 28 September 2022

Please cite this article as: Mousivand M., Javan-Nikkhah M., Anfossi L., Di Nardo F., Salina M. & Bagherzadeh K., High performance aptasensing platform development through in silico aptamer engineering for aflatoxin B1 monitoring, *Food Control* (2022), doi: https://doi.org/10.1016/j.foodcont.2022.109418.

Author contributions

Maryam Mousivand: Conceptualization, Methodology, Validation, Software, Formal Analysis, Investigation, Writing – Original Draft, Review & Edition**;**

Mohammad Javan-Nikkhah: Conceptualization, Review & Editing, Supervision, Project Administration, Funding Acquisition

Laura Anfossi: Conceptualization, Methodology, Writing, Review & Editing, Supervision, Project Administration, Funding Acquisition**;**

Fabio Di Nardo: Methodology, Software, Review & Editing**;**

Matteo Salina: Methodology**;** Review & Editing

Kowsar Bagherzadeh: Methodology**,** Software, Review & Editing**;**

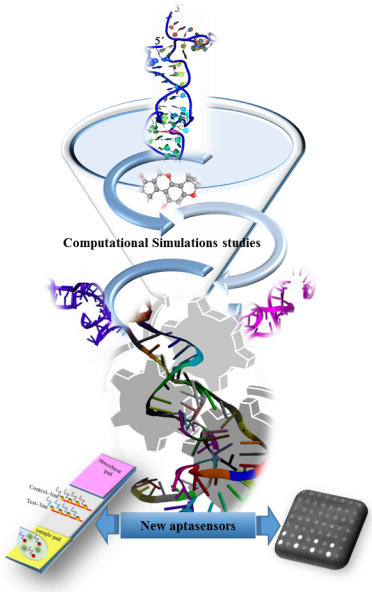

High performance aptasensing platform development through in silico aptamer engineering for aflatoxin B1 monitoring

Maryam Mousivand[*1, 2], Mohammad Javan-Nikkhah[2], Laura Anfossi[3] *, Fabio Di Nardo[3], Matteo Salina[4] and Kowsar Bagherzadeh[5,6]

1. Microbial Biotechnology Department, Agricultural Biotechnology Research Institute of Iran, Agricultural Research, Education and Extension Organization, 3135933151, Karaj, Iran

2. Department of Plant Protection, College of Agricultural Sciences & Natiral Resources, University of Tehran, 31587-77871, Karaj, Iran.Tel: + 98 2632227608

3. Department of Chemistry, University of Turin, Via Giuria, 5, I-10125 Turin, Italy. Tel.: + 39 011 670 7846

4. Proxentia S.r.l., Milano, Italy

5. Stem Cell and Regenerative Medicine Research Center, Iran University of Medical Sciences, Tehran, Iran.

6. Eye Research Center, the Five Senses Health Institute, Rassoul Akram Hospital, Iran University of Medical Sciences, 14665-354, Tehran, Iran.

Corresponding authors email: Maryam Mousivand (mmousivand93@ut.ac.ir) & Laura Anfossi (laura.anfossi@unito.it)

Abstract

Due to the technical challenges of small binding aptamer development, reliable computational simulation studies can be considered as effective tools to design novel and high functional mycotoxin aptameric probes. Here, two novel aflatoxin B1(AFB1) binding aptamers were successfully exploited as recognition elements in the lateral flow aptasensors and the reflective phantom interface (RPI) platform. Using the parent aptamer previously designed through genetic algorithm based in silico maturation (ISM) strategy, F20, a new variant, F20-T, was obtained here via coupling truncating strategy and computational simulation approaches. Two aptamer-gold nanoparticle strip biosensors were developed based on the designed probes for the simple and rapid detection of AFB1 in competitive format. The F20-based strip was more sensitive than that exploiting the truncated aptamer, with limits of detection (LOD) of 0.1 and 0.5 ng/mL, respectively. Based on the in silico and experimental selectivity evaluations of both test strips towards other mycotoxins, including aflatoxin B_2, M_1, G_1, G_2, Ochratoxin A and Zearalenone, F20-T based test strip revealed higher selectivity for AFB1. Both developed aptasensors successfully detected AFB1 in maize flour within 30 min using a simple strip reader. Exploiting of F20 and F20-T aptamers in an exclusive technology called RPI platform led to successful AFB1 detection, as well. Both designed aptameric probes can be regarded as potential recognition elements to develop screening tools for rapid, low cost and on-site AFB1 detection. Our findings highlighted the

reliable and robust application of computational simulation studies for novel small binding aptamer development and consequently open up a much-needed avenue to design various aptasensing platforms in green and cost effective ways.

Key words: aptasensor**,** computational simulations, lateral flow, aflatoxin B1, small molecule

Introduction

Among aflatoxin contaminations, AFB1 is the most prevalent and identified as the first hazard class by the International Agency for Research on Cancer (IARC, 2000). To monitor the low permissible concentrations of AFB1 in complex food and feed matrices (EC, 2010), various analytical methods have been developed. In spite of high sensitivity and specificity of chromatography based instrumental techniques, high cost, time-consuming and requiring highly skilled personnel are the main obstacles for their large-scale applications (Miklos et al., 2020). Regarding to the rapidity and simplicity, antibody-based immunoassays are widely used in routine food analysis. Considered as non- immunogenic compounds, the antibody generation for mycotoxins has several issues in terms of high cost, time consume and laborious (López-Puertollano et al., 2018).

Responding to increasing demand for affordable, accurate and simple devices for mycotoxin detection especially outside the laboratory, various biosensing platforms have been developed as alternative analysis tools to ensure food safety (Chauhan et al., 2016).While antibodies have become the most popular recognition elements in biosensor words for four decades (Di Nardo et al., 2021), aptamers have emerged as a potent rival of antibodies owing to inherent advantages over them .Unlike antibodies, aptamers can be selected over various targets regardless of their immunogenicity through an in vitro selection process called systematic evolution of ligands by exponential enrichment (SELEX). The low cost, ease of synthesis, prolonged shelf-life and regeneration under a broad range of conditions make aptamers as attractive candidates to incorporate in mycotoxin biosensing devices (Yang et al., 2013).

Despite the increasing demand for mycotoxin binding aptamers, a set of technical challenges are still the main bottlenecks for their research and commercialization. The SELEX process, known as a gold-standard methodology for aptamer development, is still cost, laborious and time-consuming. Also, the limitation of initial library diversities and sequence bias during

iterative PCR reduced the success rate of SELEX by 50% for recovering high binding affinity aptamers (Sun and Zu, 2015). These drawbacks are more highlighted in the case of small molecules binding aptamers because most affinity binding assays are not sensitive enough to separate small target-bound sequences from other ones due to drastic different size between small molecules such as mycotoxins and their binding aptamers (Ruscito and DeRosa, 2016). Also, the limited functional groups in small molecules decrease probability of finding high functional aptamers that can interact with the target via electrostatic, H-bonds, hydrophilic or π-π-stacking interactions (Mascini, 2009).

Despite the requirement of high affinity and novel aptamers to design mycotoxin biosensing platforms, a few aptamers have been developed for the class of hazardous compounds (McKeague et al., 2015). Duo to the very few novel aptamers for mycotoxins, coupling them to the various transducer systems can be considered as a compensatory solution to design high performance mycotoxin biosensing devices (Yang et al., 2013). Among various aptasensing platforms, lateral flow based aptasensor development can be considered as a promising answer to the increasing demand for simple, low cost, portable and on site detection of AFB1. However, until now a few lateral flow based aptasensors have been developed for AFB1 monitoring (Shim et al., 2014, Zhu et al., 2017, Zhang et al., 2018b, Zhao et al., 2020), all of which have exploited Apt1 aptamer patented by Neoventures Biotechnology Inc. (NeoVentures Biotechnology Inc.). Exploiting the only AFB1 aptamer (Apt1) in almost all developed aptasensors (Jia et al., 2019) makes it necessary to design novel aptamers as new recognition elements for existing biosensing platforms.

Being as main components, the bioreceptor and transducer properties have critical effects on the biosensor sensitivity and selectivity. Recently, various modified enzyme, recombinant antibody fragments and nanobodies have been developed through bioengineering techniques to increased acceptance and commercialization of the biosensing platforms (Hock et al., 2002). However, the technical barriers of aptamer development especially for small molecules have constituted major bottlenecks for aptamer engineering research and high functional aptamer discovery (Crivianu-Gaita and Thompson, 2016).

To overcome the challenges, experimental findings can be combined to the in silico approaches to refine the affinity and specificity of mycotoxin binding aptamers. Recently, aptamer engineering with the aim of sequence or scaffold optimizations have gain attentions as a promising area of active research to design and discover the novel mycotoxin binding

aptamers (Mousivand et al., 2020; Ciriaco et al., 2020; Hasegawa et al., 2016). In the case of small molecule targets, sequence truncating strategy can be considered as an effective approach to improve aptamer affinity and specificity via different size reduction between them and their aptameric partners (Aissa et al., 2020). Due to the cost and time constraints, the experimental evaluation of all designed aptamers can be considered as an important limitation for small molecules binding aptamers developing. Reliable computational simulations have the capacity to virtually screen a large database of aptamers and clarify their binding modes in cost and time effective ways (Zhang et al., 2018a; Mousivand et al., 2021; Chushak and Stone, 2009).

The aim of our study was to design new aptasensing platforms via in silico engineered aptamers instead of exploiting the same aptameric probe in different transducer systems. Therefore, F20 aptamer, previously designed based on Apt1 sequence through genetic algorithm based ISM approach (Mousivand et al., 2020, 2021), has been applied to develop a new truncated AFB1 aptamers, F20-T, via coupling truncating strategy and computational simulations. Both new designed AFB1 binding aptamers were exploited as new recognition elements in nanogold-based lateral flow aptasensors and RPI platform for AFB1 detecting.

2. Material and Methods

2.1. Computational Studies

2.1.1. Aptameric probes

The main aptameric probe, F20, was previously designed based on the Apt1 sequence (Patent: PCT/CA2010/001292) subjected to generate the second probe, F20-T, through coupling truncating strategy and computational studies as follow.

The Kd values of F20, F20-T and Apt1 were estimated through unmodified AuNPs-based colorimetric assay (details in the Supporting Information) according to Mousivand et al.(2020).

2.1.2. Library generation and secondary structure analysis

Based on F20 sequence, different variants were constructed using truncating strategy. The created library contained oligonucleotides variable in length, randomly truncated at either the 5', 3' or both end of sequences. The secondary structures of potent aptamers in the truncated

library were predicted using the Mfold web server at 37°C and at ionic concentration of 1 M of Na^{+}, 0 M of Mg^{2+} based on the free energy minimization algorithm (Zuker, 2003).

2.1.3. Molecular docking technique

Virtual screening of the truncated library was performed using AutoDockTools (ADT) 1.5.4 package (Morris et al., 2009) to evaluated AFB1 binding affinity of individual aptamers. The crystal structures of AFB1 was obtained from the PubChem database and considered as a flexible ligand while the predicted 3D-structure of aptamers were kept as rigid receptors. Three dimensional modeling of truncated ssDNA aptamer was constructed through a sequentially pipeline according to Mousivand et al. (Mousivand et al., 2020). Accordingly, different complexes were ranked based on the obtained docking scores including binding energy, type of favorable interactions and the binding sites. The best aptamer was then compared to the parent aptamer, F20, in terms of selectivity over different mycotoxins including AFB1, AFB2, AFG1, AFG2, AFM1, ZEN and OTA using molecular docking technique. The selected aptameric probe was further evaluated with the aid of molecular dynamic simulations.

2.1.4. Molecular dynamic simulations (MDs)

The conformational changes and binding mode of F20 and the corresponding truncated form, F20-T, were simulated alone in water and in complex with AFB1 during 50 ns of MD stimulations. All simulations were conducted using GROMACS 5.1.4 software package (Berendsen et al., 1995) under AMBER99SB force field (Perez et al., 2007). SwissParm web server (Zoete et al., 2011) was employed to generate the ligands topology and parameter files. The best ranked complex taken from docking results was immersed in the center of a dodecahedron periodic box containing TIP3P water model with 1 nm away from each wall. After the MDs settings according to Mousivand el al., (2021), the system went through a final 50 ns MD simulations at constant pressure and temperature conditions and the coordinates of the complexes were recorded every 10 ps for the subsequent analysis. MD simulations were analyzed using GROMACS tools and all visualizations were performed via Discovery Studio v3.5 (Biovia, 2015), VMD (Humphrey, 1996) and PyMOL (De Lano, 2002) softwares.

2.1. 5. Binding free energy MM-PBSA calculation

To estimate the binding affinity over AFB1, the molecular dynamic trajectory files of F20 and F20-T complexes were subjected to MM-PBSA analysis using g_mmpbsa tool (Kumari

et al., 2014). Gibbs free energy and its different components including electrostatic, van der Waals, polar solvation and non-polar solvation energies were estimated. Regarding to the interest in relative binding of the selected aptamers, the entropy was not calculated. The most important nucleotides involved in binding affinity toward AFB1 were retrieved through energy decomposition per residue as well.

2.2. Experimental studies

2.2.1. Reagents and Apparatus

Gold (III) chloride trihydrate (ACS reagent), bovine serum albumin (BSA), Tris-(2-carboxyethyl) phosphine hydrochloride (TCEP), and mycotoxin standard solutions were purchased from Sigma-Aldrich (St. Louis, MO, USA). All other chemicals were obtained from VWR International (Milano, Italy). 96-Microwell transparent plates were purchased from Nunc (Roskilde, Denmark). Thiol-modified aptamers and biotin modified probes were synthesized by TAG Copenhagen A/S (Denmark) (Supplementary Information, Table S1). The cellulose fiber pads (sample and absorbent pads) and nitrocellulose membranes (HF180 plus card, 60mm × 300 mm) were obtained from Millipore (Billerica, MA, USA). Test and control lines were loaded on the nitrocellulose membrane by means of an XYZ3050 platform (BioDot, Irvine, CA, USA), equipped with two BioJet Quanti^{TM} 3000 Line Dispenser for noncontact dispensing. The membrane was cut into 4.6 mm test strips by a CM4000 guillotine (BioDot, Irvine CA, USA). The color intensity of test and control lines were *scanned and then analyzed by QuantiScan 3.0 software (Biosoft, Cambridge, UK). The ultra-pure water used throughout all experiments obtained by a Milli-Q system at 18.2 MΩ.*

2.2.2. Preparation of gold nanoparticles (AuNPs)

The synthesis of ~ 30-nm-diameter gold nanoparticles was performed through the $HAuCl_4$ reduction with sodium citrate (Cavalera et al., 2020). Typically, 1 mL of 1% sodium citrate was added to 100 mL of boiling 0.01% tetrachloroauric acid under constant stirring and heating. When the suspension color changed from light yellow to deep red, heating was continued for another 10 min and then cooled to room temperature. The prepared gold nanoparticle size was confirmed through displaying a λ_{max} equal to 525 nm by UV-Visible spectrometry. The AuNPs solution was adjusted to pH 8.5 and concentrated to 10X at 14000 rpm for 10 min and then stored at 4°C for subsequent conjugation.

2.2.3. Preparation of gold nanoparticles-aptamer conjugates (AuNPs-Apt)

To activate the modified aptamers, 2 μL of 0.125 mM acetate buffer (pH 5.2) and 1.5 μl of freshly prepared 10 mM TCEP were added to 10 μL of 100 mM thiolated aptamers and incubated for 1h at room temperature. Subsequently, 500 μL of concentrated gold nanoparticles was transferred to the TCEP-treated aptamers and left reacting for at least 16 h in the dark at 4°C. After adding 10 μL of 0.25 mM tris acetate buffer (pH 8.2), the suspension was aged through adding 50 μL of 1 M NaCl dropwise (5 μL every 20 min) and left for another over night at 4°C. The prepared suspension was centrifuged at 10000 rpm for 10 min at 4°C and then resuspended in 200 μl of 25 mM tris acetate buffer (pH 8.2) containing 100 mM NaCl. After centrifugation at the same condition, the pellet was resuspended in 500 μL of 25 mM tris acetate buffer (pH 8.2) containing 300 mM NaCl and stored at 4°C (Liu and Lu, 2006).

With the aim of increasing conjugate stability, different final concentrations of aptamer F20 and F20-T (0.2, 0.5, 1, 2 and 3 μM), incubation time (4 and 24 h) and two conjugate preservation buffer composition including (i) tris acetate buffer (25 mM, pH 8.2) containing 300 mM NaCl and (ii) borate buffer (20 mM, pH 8) containing 1% BSA, 2% sucrose, 0.25% Tween 20 and 0.02% NaN_3 were further investigated.

2.2.4. Preparation of the test strip

The biotinylated DNA probes 1 and 2 were immobilized on the nitrocellulose membrane to form test and control lines, respectively, at a distance of 4 mm from each other. Prior to loading, 50 μL of the biotinylated DNA probe (100 μM) was mixed with 250 μL of 2 mg/mL streptavidin in PBS buffer (0.01 M, pH 7.4). After incubating the suspension at 4°C for 1h, 700 μL of PBS buffer (0.01 M, pH 7.4) was added. The membrane was kept at room temperature for 5 min and dried at 37 °C under vacuum for 45 min. The sample and absorbent pads were pasted on the bottom and top of the nitrocellulose membrane respectively with 1−2 mm of overlap and the prepared master card was cut into 4.6 mm test strips.

The minimum required DNA probes 1 and 2 were evaluated through developing red spots on the test and control zone respectively as a function of the hybridization reaction between 1 μM of AuNPs-Apt (F20 or F20-T) and various concentrations of both DNA probes (5, 15, 30, and 60 μM). After initial optimization, four nitrocellulose membranes with different concentrations of DNA probes 1 and 2 (100 nM, 500 nM, 2.5 μM and 5 μM) were prepared

and the color intensity at the test and control lines were further evaluated in the presence of various concentrations of AuNPs-Apt conjugates. Different concentrations of both conjugates, F20 (1 μM, 0.2 μM and 0.1 μM) and F20-T (2 μM, 0.4 μM, and 0.2 μM), were determined based on the obtained results from AuNPs-Apt preparation.

2.2.5. Aptamer based lateral flow assay procedure

The performance of two designed lateral flow aptasensors for AFB1 detection were evaluated. Therefore, 20 μL of various concentrations (0-50 ng/mL) of AFB1 standard solution in methanol were mixed with 20 μL of AuNPs-Apt conjugate (at optimized concentration) in microplate wells for 10 min at room temperature. After adding 20 μL of PBS buffer (0.01 M, pH 7.4) and 20 μL 10% Tween 20, the test strips were placed into the wells and the color intensity of the lines was analyzed 20 minutes later.

The measured area of the test and control line ratio versus AFB1 concentration in three replicates was plotted to obtain a calibration curve. The IC_{50} value was calculated by AAT Bioquest program using a four parameter logistic regression model (AAT Bioquest, Inc., Sunnyvale, CA). The limit of detection (LOD) was defined as the lowest concentration which corresponded to the T/C of the blank minus three standard deviations of the blank.

2.2.6. Selectivity of lateral flow test strip

The designed test strips were evaluated and compared in terms of selectivity toward AFB1 and cross reactivity with other mycotoxins. Under the optimal conditions, the selectivity of F20 and F20-T conjugates were determined over various mycotoxins including AFB_2, AFG_1, AFG_2, AFM_1, ochratoxin A and zearalenone at the concentration of 10 ng/mL in three replicates. The ratio of the T/C for each mycotoxin was calculated, normalized according to the AFB1 result and then expressed as selectivity percentage. The obtained mean for each mycotoxin was compared between two conjugates through the independent samples t-test using SPSS v.16.0; ($P \leq 0.05$).

2.2.7. Test strip performance under methanol content

Due to the mycotoxin extraction using conventional organic solvents, the methanol interference on the DNA hybridization process occurring in the nitrocellulose membrane was studied. Therefore, 20 μL of AFB1 standard solution (10ng/mL) diluted by various concentrations of aqueous methanol (5, 10, 25, 35, 50% v/v) was mixed with 20 μL of F20 or

F20-T AuNPs-Apt conjugates in microplate wells for 10 min at room temperature. The color intensities developed at the test and control lines were scanned 20 min later and quantified.

2.2.8. Sample assay procedures

The reliability and accuracy of both designed lateral flow test strips were conducted on four reference materials of maize flour with HPLC certified concentrations of AFB1 (<LOD, 5, 11.3 and 28.9 ppb), friendly obtained from Turin University. To perform the extraction process, one gram of each flour sample was extracted with 5 mL of 70% aqueous methanol through 2 min vortexing. After 15 min of settling, 20 µL of the supernatant was applied as the sample and mixed with 20 µL of AuNPs-Apt conjugate in a microplate well for 10 min at room temperature. To optimize the performance of the competitive format, two distinct membranes loaded with 2.5 and 5 µM of DNA probes were exploited. For further improvement, the incubation time of the strip in the well increased and the developed color was scanned after 20 and 30 min of reaction, as well. To evaluate the matrix effects and possibility of obtaining false positive results, the T/C ratios of the samples 1 for both designed test strips were compared to the blank samples in their corresponding calibration curves. The calculated T/C ratios for other samples were normalized based on sample 1 value as well.

2.2.9. Aptamer Binding affinity evaluation over AFB1 via RPI technology

Aptamer F20 and its truncated form, F20-T, were applied as recognition elements in RPI platform for AFB1 detecting. To estimate the Kd values, 400 pl of the aptameric probes (10 µM) were immobilized on the microarray surface and the binding affinity was estimated in the presence of various concentration of AFB1-BSA conjugate (0.01, 0.07, 0.28. 1.09 and 4.20 µg/mL) at the fixed times. The binding affinity of F20 and F20-T aptamers toward AFB1 were simultaneously compared to the several aptameric probes including C52, C52T, G12 and H1 designed through previous study (Mousivand et al., 2020) and two antibodies under the same condition as well.

3. Results and Discussion

3.1. Truncated library construction and thermodynamic analysis

Considering the technical challenges for small molecule aptamer development, the truncating strategy was employed to design new truncated aptameric probes. The truncated library

containing 19 potent aptamers with various lengths from 10 to 40 bp generated based on the parent sequence truncation. The minimum free energy of secondary structure formation (ΔG) in the truncated library was in the range -8.01 to 1.88 Kcal/mol (Supplementary Information, Table S2). The secondary structure prediction revealed that most of the designed sequences in the library had simple hairpin loop (H-loop) structures except those of F20-30 and F20-40 that displayed internal loop and multibranch loop, respectively.

3.2. Virtual screening of AFB1 binding aptamers

To predict the binding energy and critical interacting residues, AFB1 was docked over the aptamers in the truncated library and the estimated docking scores were in the range 1.66 to 4.17. Compared to other truncated aptamers, F20-T with H-loop structure and 19 bp in length showed the highest binding affinity towards AFB1. F20-T binding pocket includes C7, A8, G15, G10 and T14 residues that interact AFB1 coumarin and carbonyl groups through hydrogen bond formation and hydrophobic interactions (Supplementary Information, Fig S1; Tables S2 & S3). Although F20-T and its parent, F20, had the same secondary structure but their modes of interaction with AFB1 were different and determined as intercalation and minor groove binding, respectively. Compared to the parent sequence, the selectivity of the truncated aptamer had been increased over all the evaluated mycotoxins except for ZEA (Supplementary Information, Table S4). Depending on the conformational changes and losing probable binding sites, the truncating strategy can lead to increase or decrease binding affinity and selectivity of designed aptameric probes.

3.3. Molecular dynamic simulations

To clarify the truncation effects on the complex structural stability, a 50 ns molecular dynamic study was contacted on F20-T –AFB1 complex and the results were compared with MDs studies of the parent sequence, F20. The system convergence during MDs timescale was confirmed via insignificant changes in potential energy (Panman et al., 2017). The conformational changes and binding interactions of F20-T and F20 -AFB1 complex were evaluated with respect to the lone aptamer during 50ns of MDs. Regarding to the flexible nature of nucleic acids, all trajectory analysis were performed for both all atoms aptamer and its binding pockets as suggested by other study (Sharma et al., 2009). Similar to F20 aptamer, the structural stability of F20-T increased after interacting with AFB1 and the corresponding Root Mean Square Deviation (RMSD) and Root Mean Square Fluctuation (RMSF) values revealed a decreasing trend compared to the lone aptamers during MDs (Supplementary

Information, Table S5&S6 Fig. S2&S3). Visualization of trajectory files showed that AFB1 inserted between consecutive base pairs in the stem region of F20-T and subsequently the radius of gyration (Rg) values increased for all atoms and binding pockets (Supplementary Information, Fig S4). While AFB1 recognized F20 aptamer through minor groove edges of C17 and T28 residues and interacted with the binding pocket as a pseudo base subsequently leading to increase compactness and structural stability along with reduction in Rg value (Fig. 1).

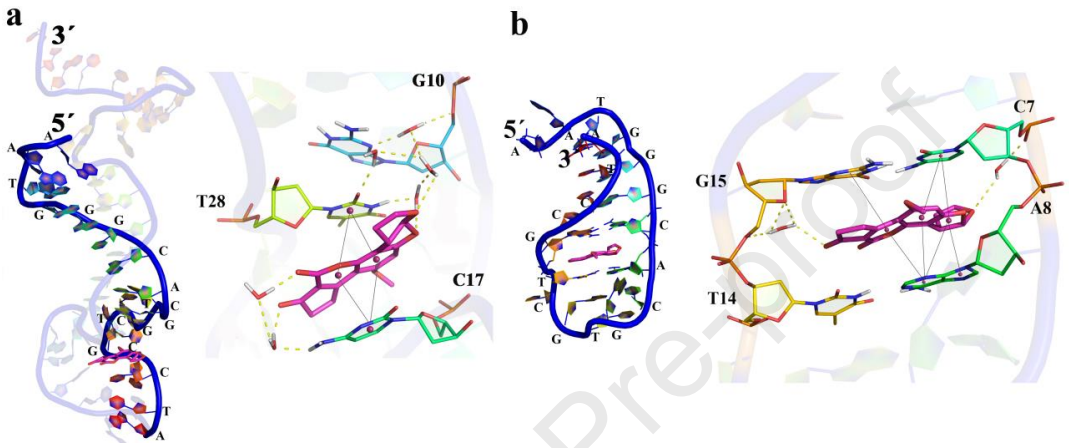

Figure 1. The molecular dynamic simulation results of F20 (a) and F20-T (b) - aflatoxin B1 complexes and residues involved in binding interaction in 3D representation. Yellow dash lines represent conventional hydrogen bonds, purple dots and the lines represent electrostatic and hydrophobic interactions, respectively. The truncated segment of the parent aptamer (a) has been highlighted in bold blue color.

The hydrogen bond formation between the aptameric probes and AFB1 along with water intermediate interactions was evaluated to determine their role in the complex stability during MDs. The average H-bonds monitored between truncated aptamer and AFB1 was approximately 7 times higher than that of F20-AFB1 complex and estimated as 0.28± 0.59. Although both aptamers mainly interacted with AFB1 through dynamic hydrogen bonds, H-bonds formed with F20-T seem to be more stable. According to the hydrogen bond occupancy percentage ≥10 ns, the only stable interaction explored in the binding pocket of the truncated aptamer with residue G15 was estimated as 15.5% (Supplementary Information, Table S7). The dynamic H-bonds between the surrounding water molecules with the binding pocket and AFB1 in F20-T complex as well as F20 complex play a key role in the structural integrity through hydrating of DNA and ligand (Supplementary Information, Table S8) as suggested by other study (Dolenc et al., 2005).

3.4. MM-PBSA calculations

The obtained MDs trajectories of F20/F20-T and AFB1 complexes were analyzed to estimate their free binding energies and different components. The binding affinity of AFB1 for the truncated aptamer is reduced by half compared to the parent sequence but it was equivalent to that of Apt1 aptamer (Mousivand et al., 2021) and estimated as -47.44 KJ/mol. According to the free binding energy component inspection, Van der Waals, non-polar and electrostatic interactions showed the major contributions to complex stability in both aptameric probes, respectively. The negative effect of polar interactions in free solvation energy can be attributed to the hydrophobic nature of AFB1 (Table 1). This finding was in line with other studies that confirmed the destabilizing role of polar interactions in binding affinity over AFB1(Mousivand et al., 2021; Almedia et al., 2018). In concordance with the docking studies, per-residue energy decomposition analysis revealed that residues C7, A8, C9, G10, T14, and G15 are the key interacting nucleotides in F20-T binding pocket over AFB1, respectively (Supplementary Information, Fig. S5). Also, the high consistency between experimentally determined binding affinity (Ka) values of F20 (3.55×10^{-5} nM), Apt1 (1.30×10^{-5} nM) and F20-T (1.12×10^{-5} nM) over AFB1 with their free binding energies estimated as -70.04, -48.67, and -47.44 KJ/mol highlighted the in silico approaches as promising tools for functional aptamer designing.

Table 1. Comparison of the free binding energy components for the aptamer-AFB_1 complexes obtained from MM-PBSA method given in KJ/mol.

aptamers	ΔE_{vdw}	ΔE_{elec}	ΔG_{polar}	$\Delta G_{non\text{-}polar}$	$\Delta G_{binding}$
F20-T	-40.44±3.67	-8.90±5.50	20.44±30.87	-15.58±5.66	-44.47
F20	-37.37±4.04	-17.13±10.92	-2.78±34.66	-12.75±1.42	-70.04
Apt1	-48.34 ± 3.67	-11.90 ± 5.50	23.44±30.87	-11.88±5.66	-48.67

3.5. Development of the aptamer-based lateral flow test strip

The principle of the designed test strip was relied on the competition between the DNA probe 1 immobilized on the test line and AFB1 to react with AuNPs-aptamer conjugate in the sample as shown in Scheme 1. As it was expected for a competitive format, the color intensity of the test line was inversely proportional to AFB1 concentration in the samples. Regardless the presence or absence of AFB1, the excess AuNPs-aptamer conjugates were captured through the linker complementary DNA probe 2 in the control line to valid the detection process and normalize strip-to-strip variation. In spite of conventional use of BSA

in the lateral flow test strips to block the non specific binding sites (Molinelli et al., 2008; Xu et al., 2010), the high binding affinity of BSA over AuNPs-aptamer conjugates and hybridization interference in the test and control lines hindered the treatment of nitrocellulose membranes with BSA. This finding was in line with results of other research that reported that the BSA binds the citrate-stabilized gold nanospheres through an electrostatic attraction via the lysine residues (Brewer et al., 2005) or by a thiol ligand exchange reaction with the unpaired cysteine residue (Tsai et al., 2011).

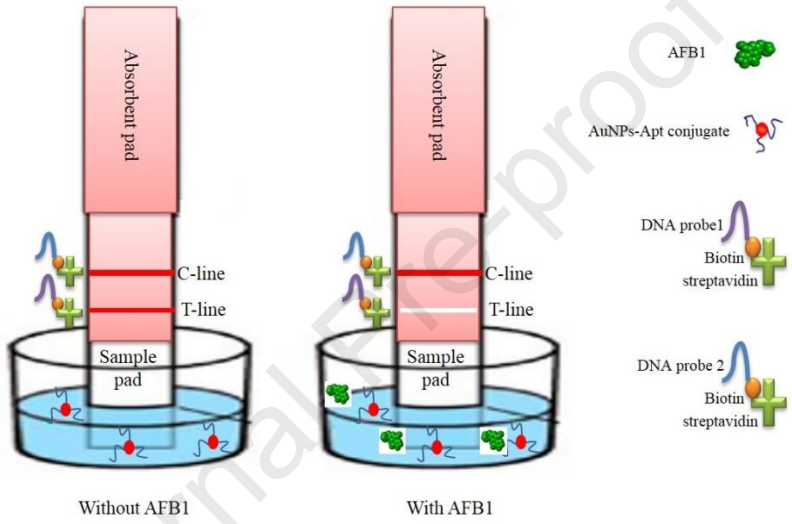

Scheme 1. Schematic illustration of aptamer-based lateral flow strip for aflatoxin B1(AFB_1) detection and result interpretation in the presence or absence of AFB1.

Difficulty in standardizing the amount of AuNPs-aptamer conjugates caused strip-to-strip variation even at a constant target concentration. To overcome this problem, the conjugates were mixed with the sample before performing the test instead of pre-adsorbing on the conjugated pads (Molinelli et al., 2008). Also, normalization can be achieved via some data corrections through using the control line intensity due to its association with variability of the gold conjugate amount and any other factors affecting the detection procedure. Therefore, the color intensity of the control line was exploited to normalize the result variations by dividing the test line area (T) by the control line area (C) (Anfossi et al., 2010). To obtain the normalized standard curve, the optimized concentration of AuNPs-aptamer conjugates was mixed with different AFB1 concentrations before the detection process on the test strip and then the T/C ratio was measured. According to the obtained results, the designed lateral flow based on F20 and F20-T aptamers showed IC_{50} of 2.9 and 15.4 ng/mL, and a dynamic range

of 0.1-50 and 0.5 -50 ng/mL, respectively. Based on the estimated LOD, the parent aptamer (0.1 ng/mL) was more sensitive compared to its truncated form (0.5 ng/mL) and showed wider T/C ratios over different AFB_1 concentrations as well (Fig. 2). The better performance of F20 based strip can be attributed to the longer length of the parent aptamer, which provides higher gold surface coverage and more stable conjugate formation. Compared to Apt1 based lateral flow strip with a quantitative LOD of 1.05 ppb (Zhang et al., 2018b), both designed lateral flow strips were able to detect AFB1 more sensitively and accurately. The high consistency between the experiments and in silico findings highlighted the reliability of the computational simulation techniques in the search of functional aptamers to be exploited for biosensor development.

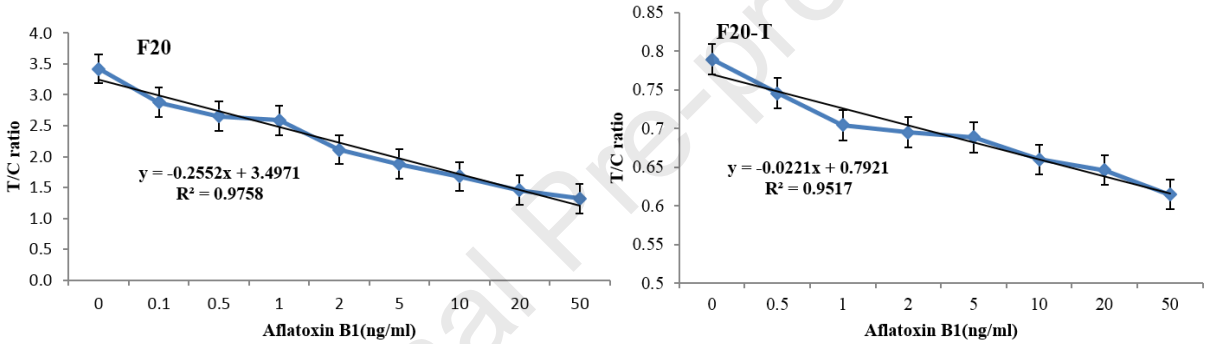

Figure 2. Calibration curves obtained by the normalized T/C ratio versus the AFB1 concentration (ng/mL) for F20-T and F20 lateral flow strips.

3.6. Optimization of the test strip components

3.6.1. Aptameric probe modifications

The load capacity of the thiol modified oligonucleotides onto the surface of Au nanoparticles can be increased due to the well-known chemical interaction between alkyl thiol and gold through Au-S bond (Love et al., 2005). Therefore, both aptameric probes had been tagged with a thiol group at the 3' during the synthesis process. In order to reduce the adsorption of the main sequence on the surface of Au-NPs and interference with the binding interaction, a poly adenine (A) spacer region between the thiol group and the aptameric sequences was designed. According to other studies, using the oligonucleotide spacer improves the hybridization efficiency and its composition and length influenced on the Au surface coverage with the functionalized oligonucleotides (Hurst et al., 2006).

3.6.2. Gold Nanoparticles-Aptamer Conjugates (AuNPs-Apt)

Despite the promoting role of NaCl in the Au/thiol interactions, it induces the gold nanoparticles aggregation during the AuNPs-Apt conjugate preparation and coloring shift from red to purple as well. Due to the protecting from salt-induced aggregation through ssDNA loading on the NPs surface (Hurst et al., 2006; Wu et al., 2018), the optimum final concentrations of F20 and F20-T based conjugates were estimated as 1 and 2 μM respectively (Supplementary Information, Fig. S6). Requiring lower parent aptamer concentration for stable conjugate preparation may be attributed to its better gold surface coverage. Also, the longer incubation time of NPs with both TCEP-treated thiol aptamers under different concentrations led to the more stable conjugate preparation. Due to the prevention of NPs aggregates, tris acetate buffer containing NaCl was identified as a better conjugate preservation buffer. Despite common use of BSA for stabilizing gold colloids conjugated to antibodies (Molinelli et al., 2008; Xu et al., 2010), the high binding affinity between citrate-stabilized gold nanospheres and BSA (Tsai et al., 2011) caused NPs aggregation during AuNPs-Apt conjugate preservation.

3.6.3. The test and control lines optimization

Regarding to the electrostatic adsorption of streptavidin on the nitrocellulose membrane and its high binding affinity to biotin, the biotinylated DNA probe-streptavidin conjugates were immobilized on the test and control lines. Owing to four identical binding sites of the streptavidin to biotin (Yuan et al., 2010), the ratio between streptavidin and the biotinylated DNA probes were set as 1:4. Under the constant concentration of both AuNPs-Apt conjugates (F20 and F20-T), the red hybridization dots were visualized for all evaluated initial concentrations of the biotinylated DNA probes and then their minimum required concentrations were estimated as 5 μM (Supplementary Information, Fig. S7). Further improvement of the test and control line performance were achieved when F20 and F20-T conjugates at their optimum concentration (0.2 and 0.4 μM, respectively) were hybridized with DNA probes 1 and 2 at the final concentration of 2.5 μM on the membrane (Supplementary Information, Fig. S8).

3.7. Test strip performance under methanol content

The adverse effects of organic solvents on the aptamer/antibody activity, colloidality of AuNPs and the co-extraction of fatty materials reduce the biosensing platforms performance

(Anfossi et al., 2010; Molinelli et al., 2009). Therefore, in the presence of a constant concentration of AFB1 (10 ng/mL), the hybridization reactions of both AuNPs-aptamer conjugates with DNA probes on the membrane were investigated under various methanol contents (5 -50 %). According to the results, the color intensities on the test and control lines gradually increased along with increasing methanol content, so that both conjugates showed the highest hybridization percentage at a concentration of methanol corresponding to 50% (Supplementary Information, Fig. S9). In contrast to earlier studies (Shim et al., 2014; Zhou et al., 2016), these findings revealed that the greater methanol content not only did not reduce DNA hybridization but increased its rate and then should be considered as an effective factor on the lateral flow responses especially in the competitive formats. These finding are consistent with those of other studies that found the hybridization rate of DNA-functionalized NPs (Smith and Liu, 2010) and molecular beacon (Dave and Liu, 2010) were significantly faster in most organic solvents compared with water attributed to the reduced activation energy barrier for the hybridization reaction in the presence of organic solvents.

3.8. The selectivity of the test strips

Both developed lateral flow strips were evaluated in terms of selectivity toward AFB1 and cross reactivity over AFB2, AFM1, AFG1, AFG2, OTA and ZEA through experimental and in silico methodologies. According to the experimental results, F20 and its truncated form based test strips showed the highest affinity towards AFB1 and a general cross reactivity over other mycotoxins. F20-T based lateral flow assay showed higher selectivity than its parent aptamer based strip toward others mycotoxins, except toward ZEA (Fig. 3). The statistical significant difference between the calculated mean selectivity of F20 and F20-T based test strips for each mycotoxin was confirmed by independent samples t-tests. In agreement with these findings, the cross reactivity of other lateral flow assays specifically designed for AFB1 have been reported, which was associated to the structural similarity of mycotoxins, especially aflatoxins (Shim et al., 2014; Zhu et al., 2018; Zhao et al., 2020).

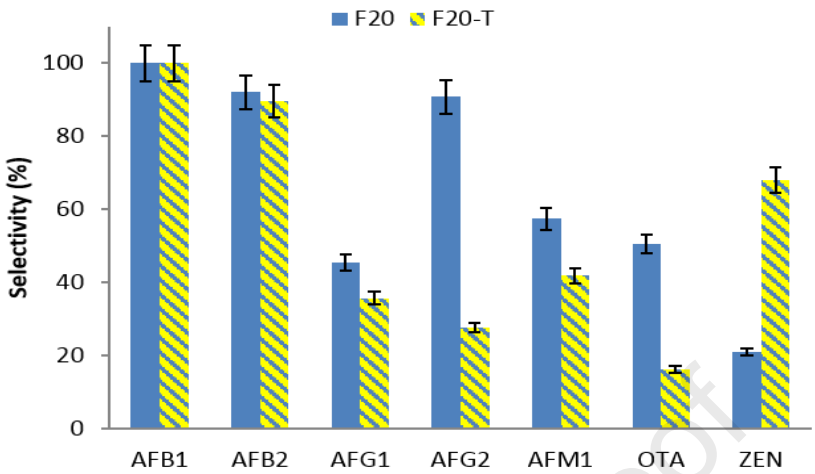

Figure 3. Selectivity of F20-T and F20 -based lateral flow strips towards various mycotoxins (10 ng/mL).

Due to the difficulty in identifying high selectivity binding probes through experimental methods (Ruscito and DeRosa, 2016), computational simulation techniques can be considered as promising approaches to find or improve probes toward a specific target (Mousivand et al., 2020). According to the docking results, F20-T showed the lower binding affinity along with the smaller binding pocket in complex with other mycotoxins except ZEA (Supplementary Information, Table S4). It seems that the higher selectivity of F20-T compared to F20 is associated with the fewer binding sites and possible conformations due to the aptamer truncation. The in silico findings were largely consistent with those experimentally obtained in terms of selectivity of the aptamers.

3.9. Real sample analysis

The accuracy of both designed aptamer based lateral flow strips were evaluated through analyzing four HPLC-certified corn flour samples. Although both F20 and F20- T based test strips were able to detect AFB1 in positive samples under optimum conditions, the parent sequence based strip was more sensitive in term of recovery percentage (Table 2). According to the results, the T/C ratios calculated for the sample 1 and the blank sample (0 ng/ml of AFB1) were relatively similar and estimated as 82.4 and 95.3 % for F20-T and F20 based test strips respectively. Therefore, the possibility of matrix interference and consequently false positive response were low in both test strips however the parent based test based strip showed more accurate results than the truncated based one.

Table 2. Recovery percentage of AFB_1 from HPLC certified corn flour samples via F20 and F20-T based lateral flow strips under optimum condition.

sample	AFB1concentration (ppb) by HPLC	Recovery % F20-T based strip	Recovery % F20 based strip
2	5	85.0	99.7
3	11.3	77.1	101.0
4	28.9	68.8	110.7

Furthermore, exploitation of the membrane prepared with lower DNA probe concentration (2.5 µM) along with longer incubation time (30 min) improved performance of both test strips likely through the improvement of competitive reactions and the reduction of matrix interference, respectively. Regarding to the pre-adsorption of extracted food matrix in the different components of the test strip (Anfossi et al., 2010), it can be interpreted that increasing the membrane incubation time enhanced the sensor performance through matrix effect management. In comparison with the truncated based test strip, all evaluated samples could be correctly ranked based on the AFB1 concentration values using F20 test strip in various experimentally condition as well (Supplementary Information, Fig. S10).

3.10. AFB1 binding affinity evaluating through RPI technology

Several surfaces were prepared by immobilizing the provided probes next to control antibodies. After fine-tuning of the microarrays which was necessary for both the deposition process and the surface preparation, microarray surface captured with RPI technology (Giavazzi et al., 2013; Salina et al., 2015). The white spots correspond to a compact single layer of molecules and the signal intensity was proportional to the mass linked to the surface. The black areas correspond to zones without bound molecules. The dissociation constants of various probes were compared through increasing concentrations of ligand (AFB1-BSA) at fixed times. According to the Kd values and width of plateaus, F20 showed the highest binding affinity over AFB1 compared to other aptameric probes estimated as 2.11 µg/mL and 83 pg/mm^2 respectively (Fig 4; Supplementary Information, Figs S11 & S12; Table S9). The lower binding affinity of F20-T compared to the parent sequence confirmed through RPI technology as well. There was a high concordance between the previous studies (Mousivand et al., 2020, 2021) and RPI technology in terms of sorting evaluated aptameric probes based on the Kd values.

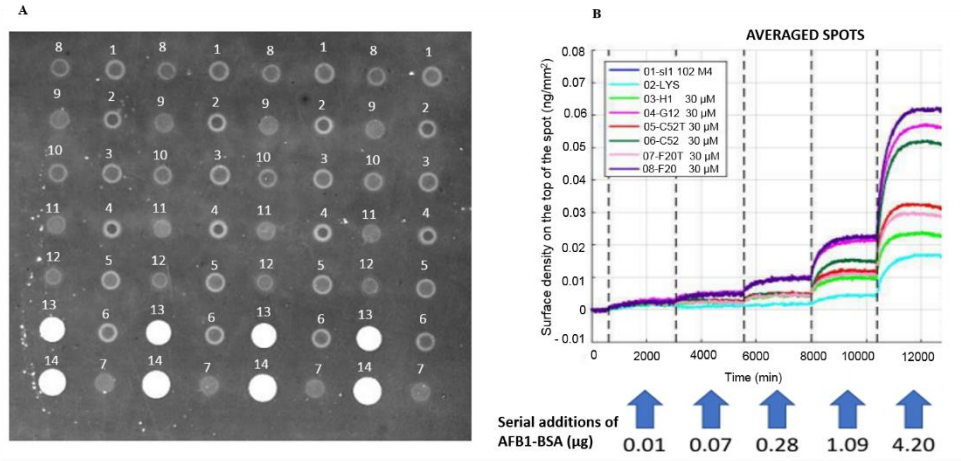

Figure 4. (A) Microarray surface captured with RPI technology under constant concentration of AFB1-BSA (12000 µg/ml); probes and their concentrations represent in numbers as follows; 1: (F20; 5 µM), 2: (F20-T; 5 µM), 3: (C52; 5 µM), 4: (C52-T; 5 µM), 5: (g12; 5 µM), 6: (H1; 5 µM), 7: (F20; 30 µM), 8: (F20-T; 30 µM), 9: (C52; 30 µM), 10: (C52-T; 30 µM), 11: (g12; 30 µM), 12: (H1; 30 µM); 13: (control antibody 1), 14: (control antibody 2); (B) The graph shows the amount of mass bounded by each type of spot over time at constant concentration (30 µM) of various aptameric probes; additions are marked with dashed lines.

Conclusion

Given the practical advantages of the aptameric probe technology over antibody generation, aptamer-based sensors can be considered as promising alternatives for accurate small molecule monitoring. However, the structural simplicity, few binding sites along with low molecular weight of small compounds are still the major bottlenecks for aptamer and aptasensing platform development for these category of compounds (Ruscito and DeRosa, 2016). As complementary options for experimentally small binding aptamer discovery, the various in silico approaches can significantly influenced their research and commercialization (Mousivand et al., 2020; Ciriaco et al., 2020). In our previous study, a well-known AFB1 aptamer sequence, Apt1, has been exploited to design a high affinity DNA aptamer, F20, through the in silico maturation strategy. Here, we integrated the truncating strategy and computational simulation studies to develop a new shorter aptamer, F20-T, based on F20 sequence. Both designed AFB1 aptamers were successfully applied as recognition elements in the lateral flow aptasensors and the RPI platform for simple and rapid AFB1 detecting. According to the legal requirements of the European Union, the sensitivity reached by both new lateral flow test strips was suitable for detecting AFB1 via strip reader. Moreover, they showed better sensitivity compared to an analogous lateral flow strip exploting the original

Apt1 (Zhang et al., 2018 b). Regarding to the high consistency between our experimental and in silico findings, aptamer engineering through sequence or scaffold refinement can be considered as a new and promising research field for novel small binding aptamer development. Low-cost integration of the newly designed probes as recognition elements in existing aptasensing platforms allow designing various novel aptasensor for small molecule target monitoring in a green way.

Acknowledgments This work was supported by Department of Plant Protection, College of Agricultural Sciences & Engineering, University of Tehran (Karaj, Iran) and Department of Chemistry, University of Turin, Via Giuria, 7 (Turin, Italy).

References

Aissa, B.S., Mastouri, M., Catanante, G., Raouafi, N., Marty, J.L.(2020). Investigation of a truncated aptamer for ofloxacin detection using a rapid FRET-based apta-assay . *Antibiotics* (Basel).9,860.

Almedia, J.S.F., Dolezal, R., Krejcar,O., Kuca,K., Musilek, K., Jun, D., França, TCC. (2018). Molecular modeling studies on the interactions of aflatoxin b1 and its metabolites with human acetylcholinesterase. Part II: Interactions with the Catalytic Anionic Site (CAS). *Toxins*.37,2041-2048.

Anfossi, L., Calderara, M., Baggiani, C., Giovannoli, C., Arletti, E., Giraudi, G. (2010). Development and application of a quantitative lateral flow immunoassay for fumonisins in maize. *Anal.Chim.Acta*.682,104e109.

Berendsen, H.J.C., van der Spoel, D., van Drunen, R. (1995). GROMACS – A message-passing parallel molecular dynamics implementation. *Comput Phys Commun*.91, 43–56.

Biovia, DS. (2015). Discovery studio modeling environment. San Diego,Dassault Systemes,Release,4.

Brewer, S.H., Glomm,W.R., Johnson, M.C., Knag, M.K., Franzen,S. (2005). Probing BSA binding to citrate-coated gold nanoparticles and surfaces .*Langmuir*.21, 9303–9307.

Cavalera, S., Di Nardo, F., Forte, L., Marinoni, F., Chiarello, M., Baggiani, C., Anfossi, L. (2020). Switching from Multiplex to Multimodal Colorimetric Lateral Flow Immunosensor. *Sensors.* 20, 6609.

Chauhan, R., Singh, J., Sachdev,T., Basu,T., Malhotra, B.D. (2016). Recent advances in mycotoxins detection. *Biosens.Bioelectron*.81, 532–545.

Chushak, Y., Stone, M. 2009. In silico selection of RNA aptamers. Nucleic Acids Research. 37: /doi.org/10.1093/nar/gkp408

Ciriaco, F., DeLeo,V.,Catucci, L., Pascale, M., Logrieco, A.F., DeRosa, M.C., DeGirolamo, A. (2020).An in-silico pipeline for rapid screening of dna aptamers against mycotoxins: the case-study of fumonisin B1, aflatoxin B1 and ochratoxin A. *Polymers*.12(12), 2983.

Crivianu-Gaita.V., Thompson, M. (2016). Aptamers, antibody scFv, and antibody Fab' fragments: An overview and comparison of three of the most versatile biosensor biorecognition elements.*Biosens. Bioelectron*.85, 32-45.

Dave, N., Liu, J. (2010). Fast molecular beacon hybridization in organic solvents with improved target specificity. *J.Phys.Chem.B* .114,15694–15699.

DeLanoW.L. (2002). An informal Newsletter associated with the BBSRC Collaborative Computational Project No. 4 on Protein Crystallography CCP4 newsletter, *On Protein Crystallography*. 40, 82e92.

Di Nardo, F., Chiarello, M., Cavalera, S., Baggiani, C., Anfossi,L. (2021). Ten years of lateral flow immunoassay technique applications: trends, challenges and future perspectives.*Sensors*.21, 51-85.

Dolenc, J., Borstnik, U., Hodoscek, M., Koller, J., Janezic, D. (2005). An ab initio QM / MM study of the conformational stability of complexes formed by netropsin and DNA. The importance of van der Waals interactions and hydrogen bonding . *J.Mol. Struct*.718,77–85.

EC. (2010). Commission regulation (EU) No 165/2010 of 26 February 2010.amending Regulation (EC) No 1881/2006 setting maximum levels for certain contaminants in foodstuffs as regards aflatoxins. Off. *J. Eur. Union* L50/8.

Giavazzi, F., Salina, M., Cerbino, Bassi, M., Prosperi,D., Ceccarello, E., Damin, F., Sola, L., Rusnati, M., Chiari, M., Chini, B., Bellini,T., Buscaglia, M. (2013). *Proceedings of the National Academy of Sciences of the United States of America*.110(23), 9350–9355.

Hasegawa, H., Savory, N., Abe,K., Ikebukuro, K.(2016). Methods for improving aptamer binding Affinity. *Molecules*.21(4), 421.

Hock, B., Seifert, M., Kramer, K. (2002). Engineering receptors and antibodies for biosensors *Biosens.Bioelectron*.17, 239–249.

Humphrey,W., Dalke,A.,Schulten, K. (1996). VMD: visual molecular dynamics. *J.Mol.Graph*.14,33–38.

Hurst, S.J., Lytton-Jean, A.K.R., Mirkin, C.A. (2006). Maximizing dna loading on a range of gold nanoparticle sizes . *Anal.Chem*.78, 8313-8318.

IARC. International Agency for Research on Cancer. Evaluation of carcinogenic risks in humans. (2002). Lyon (France): IARC. 82: 171–274.

Jia,Y., Zhou, G., Liu, P., Li, Z.,Yu, B. (2019). Recent Development of Aptamer Sensors for the Quantification of Aflatoxin B1. *Appl.Sci*. 9(11), 2364.

Kumari, R., Kumar, R., Lynn, A. (2014). g_mmpbsa - A GROMACS tool for high-throughput MM-PBSA calculations. *J. Chem. Inf. Model*.54,1951-62.

Liu, J., Lu, Y.(2006). Preparation of aptamer-linked gold nanoparticle purple aggregates for colorimetric sensing of analytes *Nat. Protoc1*.1:246–252.

López-Puertollano, D., Mercader, J.V., Agulló, C. et al. 2018. Novel haptens and monoclonal antibodies with subnanomolar affinity for a classical analytical target, ochratoxin A. Sci Rep 8, 9761. https://doi.org/10.1038/s41598-018-28138-x.

Love, J.C., Estroff, L.A., Kriebel, J.K., Nuzzo,RG.,Whitesides,G.M. (2005). Self-assembled monolayers of thiolates on metals as a form of nanotechnology. *Chem. Rev*.105(4),1103-69.

Mascini, M. (2009). Aptamers in Bioanalysis. John Wiley & Sons,Hoboken, NJ, USA.

McKeague, M., De Girolamo, A.,Valenzano, S., Pascale, M., Ruscito, A.,Velu,R., Frost, N., Hill, K., Smith, M., McConnell, E. M., DeRosa, M.C. (2015). Comprehensive Analytical Comparison of Strategies Used for Small Molecule Aptamer Evaluation. *Anal. Chem*.87, 8608−8612.

Miklós, G., Angeli,C., Ambrus, Á., Nagy, A., Kardos, V., Zentai, A., Kerekes, K.Farkas, Z.Jóźwiak, A.Bartók, T. (2020). Detection of aflatoxins in different matrices and food-chain positions. *Front Microbiol***.**11,1916.

Molinelli, A., Grossalber, K., Fuhrer, M., Baumgartner, S., Sulyok, M., Krska, R. (2008). Development of qualitative and semi-quantitative immunoassay-based rapid strip tests for the detection of T-2 toxin in wheat and oat . *J.Agric.Food Chem*. 56, 2589–2594.

Molinelli, A., Grossalber, K., Krska, R. (2009). A rapid lateral flow test for the determination of total type B fumonisins in maize . *Anal.Bioanal.Chem*. 395, 1309–1316.

Morris, G. M., Huey, R., Lindstrom,W., Sanner, M.F., Belew, R.K., Goodsell, D.S., Olson, A. J. (2009). AutoDock4 and AutoDockTools4: Automated docking with selective receptor flexibility. *J.Comput.Chem.* 30, 2785–2791.

Mousivand, M., Anfossi, L., Bagherzadeh, K., Barbero, N., Mirzadi-Gohari, A., Javan-Nikkhah, M. (2020). In silico maturation of affinity and selectivity of DNA aptamers against aflatoxin B1 for biosensor development. *Anal.Chim. Acta*.1105,178-186.

Mousivand, M., Bagherzadeh, K., Anfossi, L., Javan-Nikkhah, M. (2021). Key criteria for engineering mycotoxin binding aptamers via computational simulations: Aflatoxin B1 as a case study. *Biotechnol J*.17(2), 2100280.

Patent:PCT/CA2010/001292,NeoVentures Biotechnology Inc. 2013.Aptamer Catalogue, 24.

649 Panman,W., Japrung, D., Pongprayoon, P. (2017). Exploring the interactions of a DNA aptamer with human
650 serum albumins: simulation studies. *J.Biomol.Struct.Dyn*.35(11), 2328-2336.

651 Perez, A., Marchan, I., Svozil, D., Sponer, J., Cheatham, T.E.,Laughton, C.A., Orozco, M. (2007). Refinement
652 of the AMBER Force Field for Nucleic Acids: Improving the Description of alpha/gamma Conformers.
653 *Biophys.J*. 92, 3817–3829.

654 Ruscito, A., DeRosa, M.C. (2016). Small-Molecule Binding Aptamers: Selection Strategies, Characterization,
655 and Applications .*Front.Chem*.4,14.

656 Salina, M., Giavazzi, F., Lanfranco, R., Ceccarello, E., Sola, L., Chiari, M., Chini, B., Cerbino, R., Bellini,T.,
657 Buscaglia, M. (2015). Multi-spot, label-free immunoassay on reflectionless glass .*Biosens Bioelectron*.74, 539-
658 45.

659 Sharma, M., Bulusu, G., Mitra, A. (2009). MD simulations of ligand-bound and ligand-free aptamer: molecular
660 level insights into the binding and switching mechanism of the add A-riboswitch . *RNA*.15,1673-92.

661 Shim,W.B., Mun, H., Joung, H.A., Ofori, J.A., Chung, D.H., Kim, M.G. (2014). One-step simultaneous
662 immunochromatographic strip test for multianalysis of ochratoxin A and zearalenone. *Food Control*.36,30-35.

663 Smith, D., Liu, J. (2010). Assembly of DNA-functionalized nanoparticles in alcoholic solvents reveals opposite
664 thermodynamic and kinetic trends for DNA hybridization .*J.Am.Chem.Soc.*132(18), 6300–6301.

665 Sun,H.,Zu,Y., 2015.Molecules.20,11959-11980.

666 Tsai, D.H., DelRio, F.W., Keene, A.M., Tyner, K.M., MacCuspie, R.I., Cho, T.J., Zachariah, M.R., Hackley, V.
667 A. (2011). Adsorption and conformation of serum albumin protein on gold nanoparticles investigated using
668 dimensional measurements and in situ spectroscopic methods . *Langmuir*.27, 2464–2477.

669 Wu, S., Liu, L., Duan, N., Li, Q., Zhou,Y.,Wang, Z. (2018). An aptamer-based lateral flow test strip for rapid
670 detection of zearalenone in corn samples . *J.Agr.Food Chem*. 66,1949-1954.

671 Xu, Y., Huang, Z.B., He, Q.H., Deng, S.Z., Li, L.S., Li,Y.P.(2010). Development of an immunochromato-
672 graphic strip test for the rapid detection of deoxynivalenol in wheat and maize .*Food Chem*.119, 834e839.

673 Yang, X.H., Kong,W.J.,Yang, M.H., Zhao, M., Ouyang, Z. (2013). Application of Aptamer Identification
674 Technology in Rapid Analysis of Mycotoxins . *Chinese J.Anal.Chem*. 41(2), 297-306.

675 Yuan,Y., Yuan, R., Chai,Y., Zhuo,Y., Bai, L., Liao,Y. (2010). An electrochemical enzyme bioaffinity electrode
676 based on biotin-streptavidin conjunction and bienzyme substrate recycling for amplification *Anal. Biochem*. 405,
677 121-126.

678 Zhang,Y., Lu,T., Wang,Y., Diao, C., Zhou, Y., Zhao, L.,Chen, H. (2018a). Selection of a DNA aptamer against
679 zearalenone and docking analysis for highly sensitive rapid visual detection with a label-free aptasensor. *J.*
680 *Agric.Food Chem.*66,12102–12110.

Zhang, S., Zhao, S., Wang, S., Liu, J., Dong, Y. (2018b). Development of lateral flow immune chro - matographic strips for micropollutant screening using colorants of aptamer-functionalized nanogold particles, part ii: experimental verification with aflatoxin b1 and chloramphenicol. *J.AOAC Int*.101(5),1408–1414.

Zhao, Z., Wang, H., Zhai,W., Feng, X., Fan, X., Chen, A.,Wang, M. (2020). A lateral flow strip based on a truncated aptamer-complementary strand for detection of type-b aflatoxins in nuts and dried figs. *Toxins* (Basel)12(2),136.

Zhou, W., Kong, W., Dou, X., Zhao, M., Zhen,O., Yang, M. (2016). An aptamer based lateral flow strip for on-site rapid detection of ochratoxin A in Astragalus membranaceus .*J.Chromatogr.B.Anal.Technol.Biomed.Life Sci*. 1022,102–108.

Zhu,C., Zhang, G., Huang,Y.,Yang, S., Ren, S., Gao, Z., Chen, A.(2018). A. Dual-competitive lateral flow aptasensor for detection of aflatoxin B1 in food and feedstuffs . *J.Hazard.Mater*.344, 249-257.

Zoete,V., Cuendet,M., Grosdidier, A., Michielin, O. (2011).SwissParam: A fast force field generation tool for small organic molecules.*J.Comput.Chem*.32, 2359–2368.

Zuker, M. (2003). Mfold web server for nucleic acid folding and hybridization prediction. *Nucleic Acids Res*. 31(13).

Supplementary material

High performance aptasensing platform development through in silico aptamer engineering for aflatoxin B1 monitoring

Maryam Mousivand[*1, 2], Mohammad Javan-Nikkhah[2] , Laura Anfossi[3] *, Fabio Di Nardo[3], Matteo Salina[4] and Kowsar Bagherzadeh[5,6]

1- Microbial Biotechnology Department, Agricultural Biotechnology Research Institute of Iran, Agricultural Research, Education and Extension Organization, 3135933151, Karaj, Iran

2- Department of Plant Protection, College of Agricultural Sciences & Engineering, University of Tehran, 31587-77871, Karaj, Iran.Tel: + 98 2632227608

3- Department of Chemistry, University of Turin, Via Giuria, 5, I-10125 Turin, Italy. Tel.: + 39 011 670 7846

4- Proxentia S.r.l., Milano, Italy

5- Stem Cell and Regenerative Medicine Research Center, Iran University of Medical Sciences, Tehran, Iran.

6- Eye Research Center, the Five Senses Health Institute, Rassoul Akram Hospital, Iran University of Medical Sciences, 14665-354, Tehran, Iran.

Corresponding authors email: Maryam Mousivand (mmousivand93@ut.ac.ir) & Laura Anfossi (laura.anfossi@unito.it)

738 **Table S1.** Modified aptamers and probe sequences used in this study

aptamers/probes	sequence (5'-3')
thiol-modified aptamer F20	5'-aatgggcacgtgctgcctatatgtgtctcgtgcccttcgctaggcccactaaaaaaaaaaaaaaaaaa-SH-3'
thiol-modified aptamer F20-T	5'-aatgggcacgtgctgcctaaaaaaaaaaaaaaaaaa-SH-3'
biotin-modified DNA probe1	5'-agtgggcctagcgaagggcacgagacacatataggcagcacgtgcccatt-Biotin-3'
biotin-modified DNA probe2	5'-ttttttttttttttttt-Biotin3'
aptamer F20	5'-aatgggcacgtgctgcctatatgtgtctcgtgcccttcgctaggcccact-3'
aptamer F20-T	5'-aatgggcacgtgctgcct-3'

739

740

741

742

743 **Table S2.** The sequence, minimum free energy of secondary structure formation (ΔG), length (bp), truncated
744 direction and docking score of aptamers in the truncated library.

Aptamers	**Sequences (5'-3')**	**ΔG (Kcal/mol)**	**Length (bp)**	**Truncated direction**	**Docking score**
F20	aatgggcacgtgctgcctatatgtgtctcgtgcccttcgctaggcccact	-8.01	50	-	5.68
F20-T	aatgggcacgtgctgccta	-3.51	19	3'	4.17
F20-40-3	aatgggcacgtgctgcctatatgtgtctcgtgcccttcgc	-8.01	40	3'	3.93
F20-30	atgtgtctcgtgcccttcgctaggcccact	-1.97	30	5'	3.72
F20-17	ccttcgctaggcccact	-0.35	17	5'	3.70
F20-40	tgctgcctatatgtgtctcgtgcccttcgctaggcccact	-2.05	40	5'	3.38
F20-16	cttcgctaggcccact	0.36	16	5'	3.06
F20-18	cccttcgctaggcccact	-0.87	18	5'	2.90
F20-18-3	aatgggcacgtgctgcct	-3.51	18	3'	2.87
F20-19	gcccttcgctaggcccact	-0.89	19	5'	2.86
F20-20-3	aatgggcacgtgctgcctat	-3.66	20	3'	2.83
F20-17-3	aatgggcacgtgctgcc	-2.99	17	3'	2.72
F20-10	taggcccact	0.36	10	5'	2.45
F20-30-3	aatgggcacgtgctgcctatatgtgtctcg	-4.14	30	3'	2.39
F20-10-3	aatgggcacg	1.88	10	3'	2.03
F20-20	tgcccttcgctaggcccact	-1.50	20	5'	1.97
F20-15-3	aatgggcacgtgctg	-0.82	15	3'	1.94
F20-16-3	aatgggcacgtgctgc	-1.15	16	3'	1.88
F20-15	ttcgctaggcccact	0.36	15	5'	1.85
F20-30-3-5	tgctgcctatatgtgtctcgtgcccttcgc	-0.05	30	5' & 3'	1.66

745

746

747

748 **Table S3**. Principal interactions between residues of the truncated aptamers with AFB1.

Aptamers	Carbone and conventional hydrogen binding	Hydrophobic interaction	Electrostatic interaction
	H-Donor-H-Acceptor	Pi-Orbitals- π/ σ /alkyl	Negative-Pi-Orbitals
F20-10	G6:H22 - AFB1:O5 G6:H22 - AFB1:O6 G6:H1 - AFB1:O6 G4:C1' - AFB1:O2 AFB1:C15 - G4:N3 AFB1:C17 - G4:O3'	G4:C2' - AFB1-π-σ G4 - AFB1/π-alkyl G4 - AFB1/π-alkyl	
F20-15	G10:C5' - AFB1:O4 U11:C6 - AFB1:O3 AFB1:C15 - G12:OP1	U11 - AFB1/π-alkyl	
F20-16	AFB1:C17 - C9:O2 G5:H21 - AFB1:O6	A8 - AFB1/ π- π	G6:OP1 - AFB1/ π-anion
F20-17	G6:H21 - AFB1:O5 AFB1:C15 - G4:O3' G5:H21 - AFB1:O6 G6:H21 - AFB1:O5	G5 - AFB1/ π- π G5 - AFB1/ π- π	
F20-18	AFB1:C15 - G4:O3' AFB1:C17 - G5:O3' A8:H61 - AFB1:O5 A8:H61 - AFB1:O6	C7 - AFB1/ π- π T14 - AFB1/ π- π	
F20-19	AFB1:C15 - G10:O6 AFB1:C17 - G15:OP2 G4:H21 - AFB1:O4 G5:H21 - AFB1:O1 AFB1:C15 - G6:N3	T14 - AFB1/ π- π C7 - AFB1/π-alkyl A8 - AFB1/π-alkyl G5:C1' - AFB1/ π-lone pair G5:O4' - AFB1/ π- π G5 - AFB1/ π- π	
F20-20		G5 - AFB1/ π- π G5 - AFB1/ π- π G5 - AFB1/π-alkyl G5 - AFB1/π-alkyl G6 - AFB1/π-alkyl	
F20-30	T24:H3 - AFB1:O6 G25:H21 - AFB1:O5 AFB1:C15 - T24:O3'	G25 - AFB1/ π- π	
F20-40	G4:H21 - AFB1:O1		G5:OP1 - AFB1/ π-anion
F2-10-3	A8:H62 - AFB1:O4 G3:C1' - AFB1:O2 T10:C4' - AFB1:O5	G3 - AFB1/ π- π A2 - AFB1/π-alkyl G3 - AFB1/π-alkyl	

749

750

751

752 **Table S3.** (continued). Principal interactions between residues of the truncated aptamers with AFB1.

F2-20-3	G3:H21 - AFB1 AFB1:C17 - T6:OP2 AFB1:C17 - T6:O5'	G3 - AFB1/π-alkyl T6 - AFB1/π-alkyl	C10:OP1 - AFB1/ π-anion
F2-30-3	A22:C1' - AFB1:O6	T17 - AFB1/π-alkyl A22 - AFB1/π-alkyl A22 - AFB1/π-alkyl	G19:OP1 - AFB1/ π-anion A22:OP2 - AFB1/ π-anion
F2-40-3	AFB1:C17 - T27:O4' AFB1:C17 - A38:N1	C25 - AFB1/π-alkyl C39 - AFB1/π-alkyl	
F2-30-3-5	G20:H21 - AFB1:O6 AFB1:C17 - G20:O3'	G20 - AFB1/ π- π G20 - AFB1/ π- π G20 - AFB1/π-alkyl G20 - AFB1/π-alkyl	
F2-15-3	G4:H22 - AFB1:O5 G4:H22 - AFB1:O6 G4:H1 - AFB1:O6 T2:H3 - AFB1	T1 - AFB1/ π- π	
F2-16-3	A14:H62 - AFB1:O4	AFB1:C17 - A14/ π- π G9 - AFB1/ π- π G9 - AFB1/ π- π G9 - AFB1/ π- π G9 - AFB1/ π- π	
F2-17-3	G10:H21 - AFB1:O2 A9:C1' - AFB1:O4 AFB1:C17 - T4:O3'	G10 -AFB1/π-alkyl G11 -:AFB1/π-alkyl	
F2-18-3	C1:C1' - AFB1:O4 AFB1:C15 - C3:O2	C3 - AFB1/π-alkyl	
F2-19-3	G8:H21 - AFB1:O5 G8:H21 - AFB1:O6 AFB1:C3 - T10:OP2 AFB1:C17 - G8:O5' AFB1:C17 - C9:OP1	T5 - AFB1/π-alkyl	

Table S4. Binging energy, binding sites, Inhibition constant, type of interactions (number of interactions) and Ref RMSD for the best conformation of F20 and F20-T aptamers docked with AFB_2, AFG_1, AFG_2, AFM_1, OTA and ZEN.

Complex	Binding Energy (kcal/mol)	Binding sites	Inhibition constant (μm)	Type of interactions* (number of interactions)	RMSD (Å)
F20-AFB2	-9.67	T28, C27,C17,G12	1.58	Hb(12)+E(6)+O(1)	19.2
F20-AFG1	-5.85	C27,T28,C29,G10,G12,C17	18.28	Hg(4)+Hb(8)+O(1)	21.18
F20-AFG2	-7.0	C27,T28,C29,G10,G12,C17	5.24	Hg(3)+Hb(9)+O(1)	21.43
F20-AFM1	-4.3	C27,T28,C29,G10,G12,C17	562.62	Hg(6)+Hb(2)+O(2)	31.75
F20-OTA	-5.72	C27,T28,C29,G10,G12,C17,C16	39.26	Hg(9)+Hb(13)+O(1)	23.15
F20-ZEN	-5.41	G4,G6,T37	90.55	Hg(3)	24.33
F20-T-AFB2	-8.0	G15,C12,C7, A8,T14	1.38	Hg(1)+Hb(4)+E(8)	21.86
F20-T-AFG1	-4.82	G15,C7, A8,T14	290.86	Hb(6)+E(1)	23.28
F20-T-AFG2	-4.73	G15,G10,C7, A8,T14	343.2	Hg(4)+Hb(6)	24.35
F20-T-AFM1	-4.29	G5,G6,G15,C7	712.65	Hg(5)+Hb(1)	24.9
F20-T-OTA	-4.58	A8,G6	440.32	Hg(3)+Hb(2)	28.62
F20-T-ZEN	-5.44	C7,A8,G15	103.12	Hg(3)+Hb(3)	26.98

Hg: Hydrogen Bonding Hb: Hydrophobic Bonding E: Electrostatic O: others

Table S5. RMSD, RMSF and Rg values (nm) for binding pocket of the aptamer-AFB_1 complexes (C) with respect to the lone aptamers (F) during 50 ns molecular dynamic simulation.

aptamer	RMSD(F) (mean±SD)	RMSD (C) (mean±SD)	RMSF(F) (mean±SD)	RMSF (C) (mean±SD)	Rg(F) (mean±SD)	Rg(C) (mean±SD)
F20-T	0.42±0.04	0.31±0.04	0.24±0.03	0.15±0.02	0.78±0.2	0.81±0.2
F20	0.59±0.07	0.39±0.04	0.24±0.06	0.15±0.05	1.03±0.03	0.84±0.02

Table S6. RMSD, RMSF and Rg values (nm) for all atoms of the aptamer-AFB1 complexes (C) with respect to the lone aptamers (F) during 50 ns molecular dynamic simulation.

Aptamer	**RMSD(F)** (mean±SD)	**RMSD (C)** (mean±SD)	**RMSF(F)** (mean±SD)	**RMSF (C)** (mean±SD)	**Rg(F)** (mean±SD)	**Rg(C)** (mean±SD)
F20-T	0.48±0.07	0.40±0.08	0.24±0.07	0.14±0.05	1.19±0.03	1.28±03
F20	0.94±0.17	1.35±0.28	0.608±0.28	0.8±36	2.48±0.10	2.34±0.27

Table S7. Comparison of the hydrogen bond interactions (mean± SD) and hydrogen bond occupancy of F20-T and F20 aptamers in the complexes with aflatoxin B1during 50 ns of MD simulation

Aptamer	Donor	Acceptor	Hydrogen bond occupancy	hydrogen bond interactions (mean± SD)

			(%)	
F20-T	G10 (H21)	AFB1(O3)	4.4	0.28 ± 0.59
	G10 (H21)	AFB1 (O2)	7.2	
	G10 (H1)	AFB1 (O3)	1	
	G10 (H1)	AFB1 (O2)	15.5	
	C7(H61)	AFB1 (O5)	0.1	
F20	T28 (H3)	AFB1 (O1)	1.1	0.04±0.21
	C17 (H41)	AFB1 (O2)	0.1	
	G15 (H21)	AFB1 (O1)	0.1	
	G12 (H21)	AFB1(O6)	1.3	
	G12 (H21)	AFB1(O1)	0.5	
	G10 (H21)	AFB1(O6)	0.8	
	G10 (H21)	AFB1(O5)	0.2	
	G10 (H21)	AFB1(O4)	0.1	
	G10 (H21)	AFB1(O3)	0.2	

Table S8. Comparison of the water intermediate interactions (mean± SD) and their occupancy ranges involved with AFB1 and binding pocket of F20-T and F20 complexes during 50ns of MD simulation

Aptamer	**Water molecules-binding pocket**		**Water molecules-AFB1**	
	hydrogen bond interactions(mean± SD)	occupancy range (%)	hydrogen bond interactions (mean± SD)	occupancy range (%)
F20-T	78.42±4.75	1-5.1	2.91±1.15	0.1-1.4
F20	82.78±5.17	1-9.6	3.32±1.25	0.1-0.8

Table S9. Determination of dissociation constant (Kd) and width of plateau of F20-T, F20, C52, C52T, g12 and H1 aptamers via reflective phantom interface (RPI) technology.

Aptamers	**Kd (µg/ml)**	**Kd (nM)**	**Width of plateau**
F20	2.15	31.9	83µg/mm^2
F20-T	4.61	68.8	61µg/mm^2
C52	2.67	39.9	73µg/mm^2
C52T	3.34	52.8	58pg/mm^2
g12	2.12	31.6	78pg/mm^2
H1	3.77	56.1	45pg/mm^2

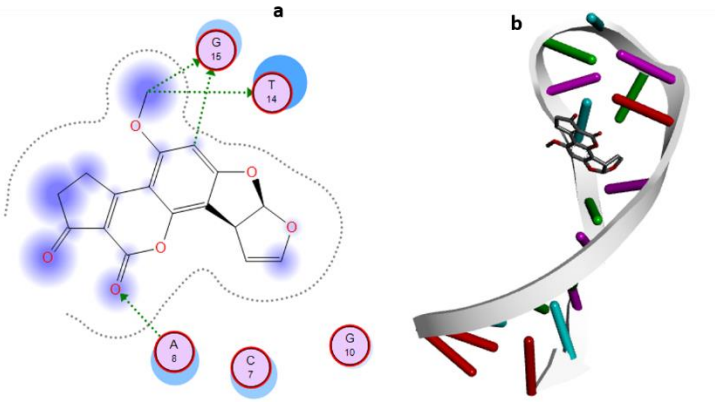

Fig. S1. The docking results of F20 -T -AFB1 complex and residues involved in binding interaction in 2D (a) and 3D (b) representation.

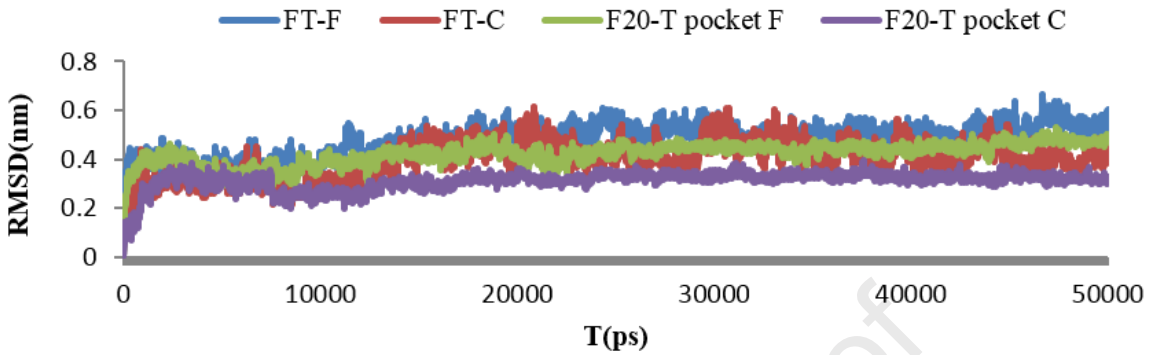

Fig. S2. RMSD plot of F20-T aptamer for all atoms (lone: Blue; in complex with aflatoxin B1: Red) and binding pocket (lone: Green; in complex with aflatoxin B1: Purple) during the simulation time.

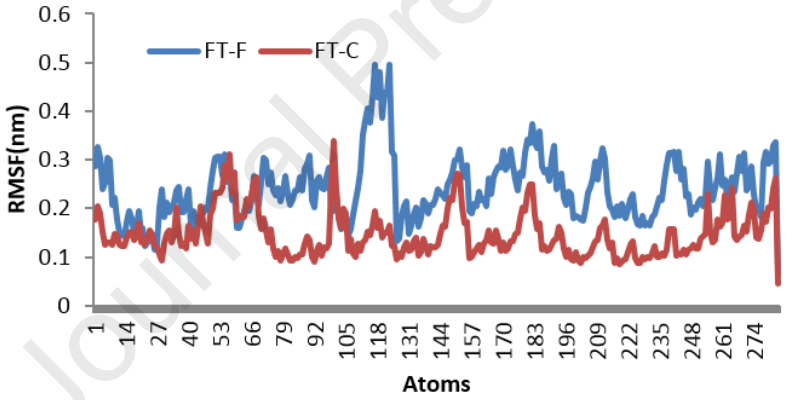

Fig. S3. RMSF plot of F20-T aptamer for all atoms (lone: Blue; in complex with aflatoxin B1: Red) during the simulation time.

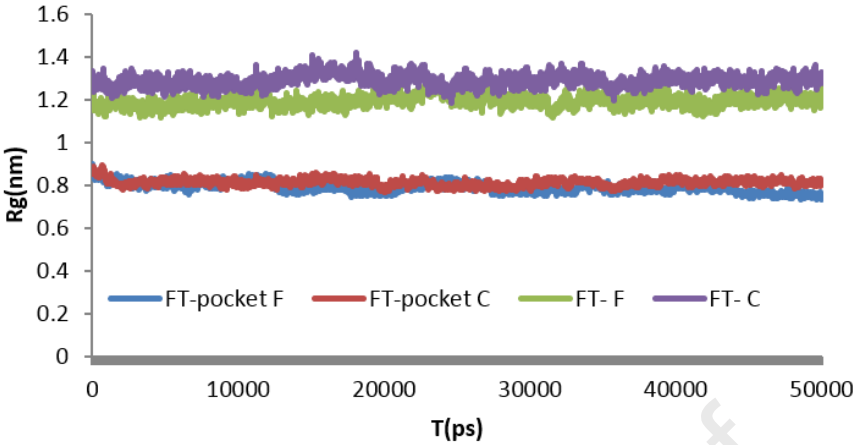

Fig. S4. Rg plot of F20-T aptamer for all atoms (lone: Green; in complex with aflatoxin B1: Purple) and binding pocket (lone: Blue; in complex with aflatoxin B1: Red) during the simulation time.

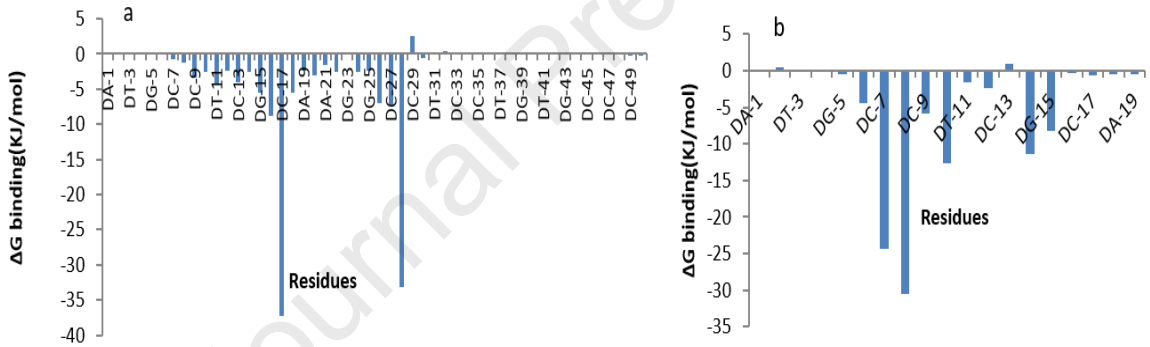

Fig. S5. Energy component decomposition analysis per F20 (a) and F20-T (b) residues interacting with aflatoxin B1 through MM-PBSA method during 50ns of MD simulation.

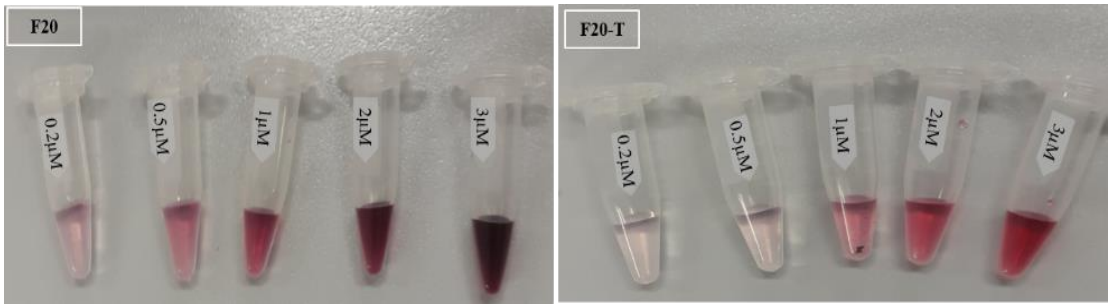

Fig. S6. Optimization of the gold nanoparticles-aptamer conjugate preparation under different concentrations of the thiolated F20 and F20-T aptamers.

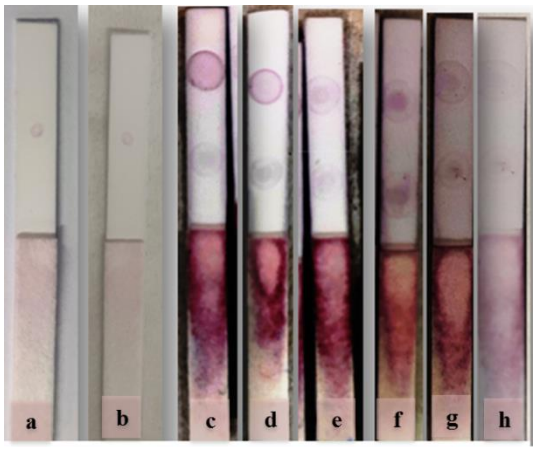

Fig. S7. Determination of the minimum required concentrations of DNA probe 1 and DNA probe 2 at the test and control lines under the constant concentration (1 µM) of F20 and F20-T ; a:(F20, 60µM), b: (F20-T, 60µM), c:(F20,30µM), d:(F20,15µM), e:(F20,5µM), f:(F20-T, 30µM), g:(F20-T,15µM), h: (F20-T, 5µM)

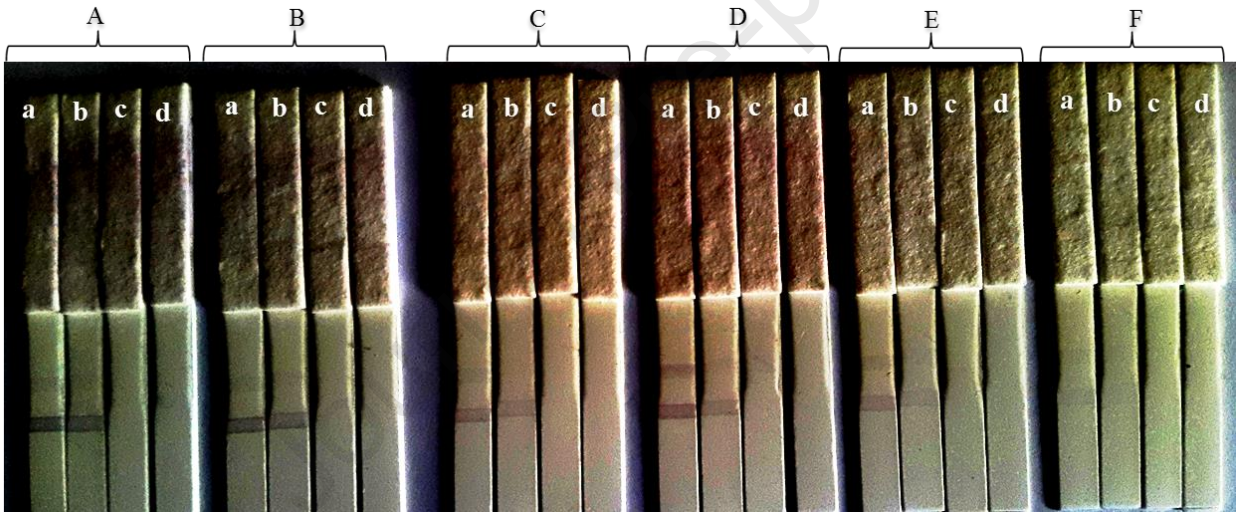

Fig. S8. Optimization of the test and control line performance using various nitrocellulose membranes with different concentrations of DNA probes 1 and 2 (**a**:100nM, **b**:500nM, **c**:2.5µM , **d**:5 µM) under different concentration of thiolated F20 (**A**:1µM ,**B**:0.2 µM , **C**:0.1µM) and F20-T (**D**: 2 µM, **E**:0.4 µM, **F**:0.2µM) aptamers.

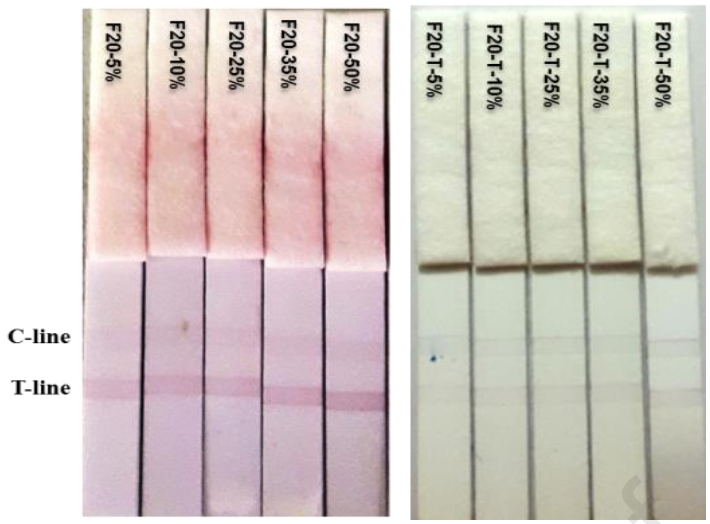

817

818 **Fig. S9**. Evaluation of the test and control line intensities of F20 and F20-T based test strips under various
819 concentrations of aqueous methanol (5, 10, 25, 35, 50% v/v) at AFB1 constant concentration (10 ng/mL).
820

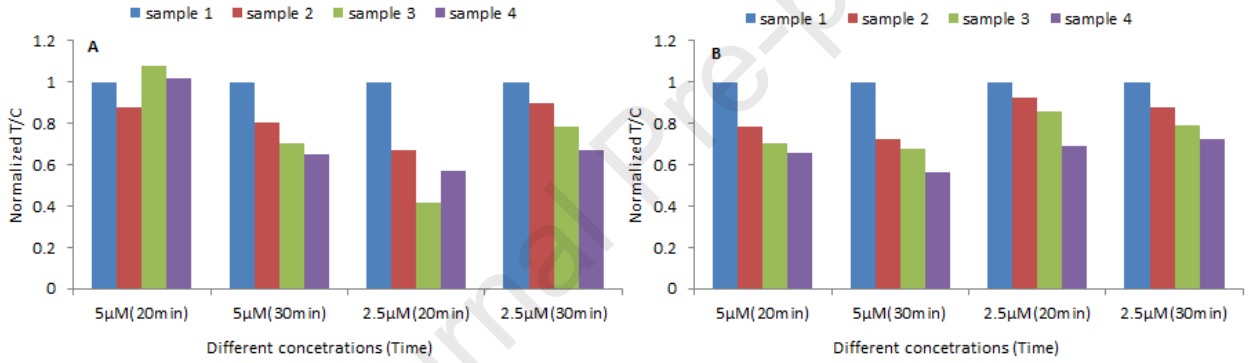

8

822 **Fig.S10**. AFB_1 detection in corn flour samples via F20 (A) and F20-T (B) based lateral flow strips under
823 different conditions including two membranes prepared with different DNA probe concentrations (2.5 and 5
824 µM) and two incubation time (20 and 30 min). AFB1 concentrations in HPLC-certified samples 1, 2, 3 and 4
825 were <LOD, 5, 11.3 and 28.9 ppb, respectively .

826

827

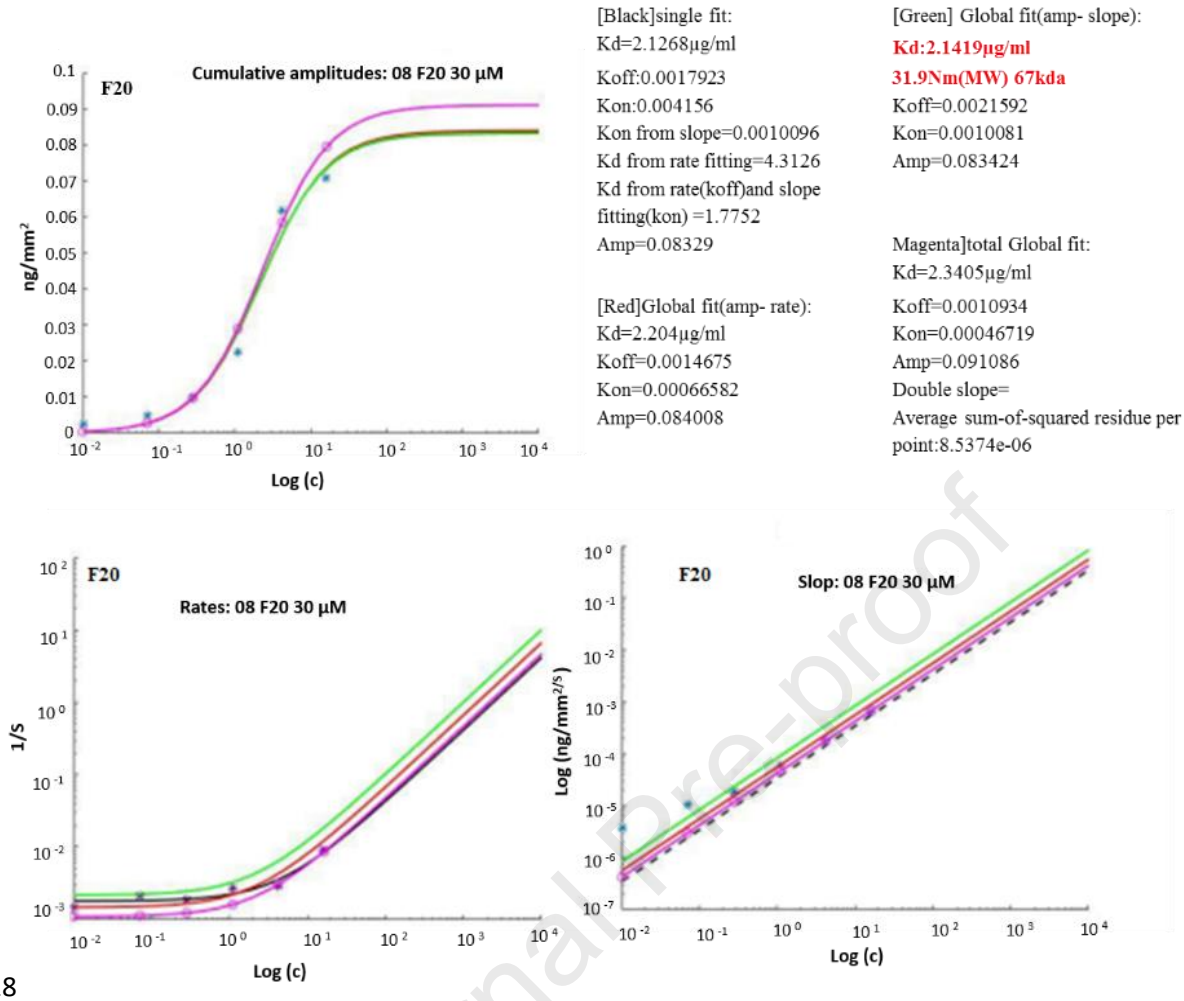

828

829 **Fig. S11**. Determination of dissociation constant (Kd) of F20 aptamer via reflective phantom interface (RPI)
830 technology.

831

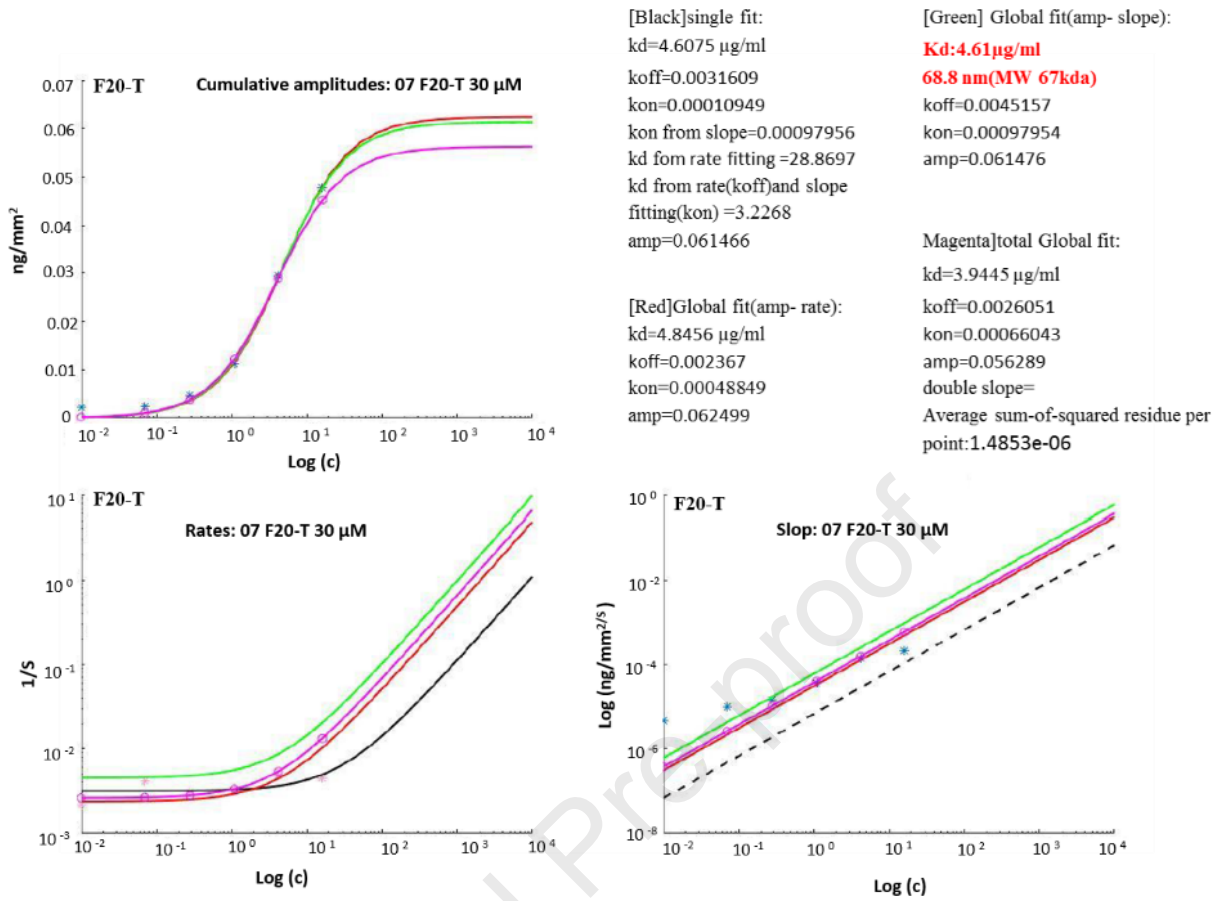

832

833

834 **Fig. S12**. Determination of dissociation constant (Kd) of F20-T aptamer via reflective phantom interface (RPI)

835 technology.

1. A new truncated Aflatoxin B1 binding aptamer was designed via in silico studies.

2. The truncated and the parent aptamer were successfully applied to build aptasensors.

3- The redesigned aptasensing platforms provided high sensitive AFB1 detection.

4- In silico engineered aptamers can be costly exploited for new aptasensor development.

Declaration of interests

☒ The authors declare that they have no known competing financial interests or personal relationships that could have appeared to influence the work reported in this paper.

☐ The authors declare the following financial interests/personal relationships which may be considered as potential competing interests: